Direct photo-etching of poly(methyl methacrylate) using focused extreme ultraviolet radiation from a table-top laser-induced plasma source

Frank Barkusky,[a] Christian Peth, Armin Bayer, and Klaus Mann
Laser-Laboratorium-Göttingen e.V., Hans-Adolf-Krebs-Weg 1, D-37077 Göttingen, Germany

(Received 21 November 2006; accepted 9 May 2007; published online 26 June 2007)

In order to perform material interaction studies with intense extreme ultraviolet (EUV) radiation, a Schwarzschild mirror objective coated with Mo/Si multilayers was adapted to a compact laser-based EUV plasma source (pulse energy 3 mJ at $\lambda = 13.5$ nm, plasma diameter ~ 300 μm). By $10\times$ demagnified imaging of the plasma a pulse energy density of ~ 75 mJ/cm^2 at a pulse length of 6 ns can be achieved in the image plane of the objective. As demonstrated for poly(methyl methacrylate) (PMMA), photoetching of polymer surfaces is possible at this EUV fluence level. This paper presents first results, including a systematic determination of PMMA etching rates under EUV irradiation. Furthermore, the contribution of out-of-band radiation to the surface etching of PMMA was investigated by conducting a diffraction experiment for spectral discrimination from higher wavelength radiation. Imaging of a pinhole positioned behind the plasma accomplished the generation of an EUV spot of 1 μm diameter, which was employed for direct writing of surface structures in PMMA. © *2007 American Institute of Physics*. [DOI: 10.1063/1.2749210]

I. INTRODUCTION

Extreme ultraviolet lithography (EUVL) can be regarded as the extension of optical lithography to shorter wavelengths and is one option for the semiconductor industry for next generation lithography (NGL) systems.[1] Using reflective imaging optics on the basis of multilayer mirrors, electronic devices with structure sizes well below 45 nm could be manufactured at a wavelength of 13.5 nm. For industrial lithographic systems EUV radiation with high average power is required, which can be generated either by laser or discharge based plasma sources. Such EUV sources and corresponding beam steering optics are currently being developed with tremendous effort.[2–4]

Besides semiconductor microlithography, there are also other applications of EUV radiation, which can strongly profit from the EUVL source and optics developments. For example, the generation of color centers in LiF crystals was demonstrated,[5] which can be used as laser-active medium,[6] for data storage,[7] or as a detector for EUV microscopy.[8]

Another application is direct structuring of surfaces by EUV photoetching, which has the potential to generate features of highest lateral resolution due to the strongly reduced diffraction limit as compared to standard higher wavelength sources. For polymers like poly(methyl methacrylate) (PMMA) this was already demonstrated by Juha *et al.*,[9] who used a contact mask for direct ablation under the influence of an intense EUV plasma, generated by a high-energy (multi-Joule) laser system.[9] Similar experiments were also conducted by Fiedorowicz *et al.*[10]

Rather than the high average powers needed for microlithography, EUV photoetching requires high EUV pulse energy densities. As in the experiments mentioned above, these can be achieved by positioning the samples close to the EUV plasma, leading, however, to radiation damage or effects caused by unwanted out-of-band radiation.

Alternatively, EUV optical elements can be employed for focusing or demagnification of the plasma. T. Makimura *et al.* used an ellipsoidal grazing incidence mirror to focus a laser-generated EUV plasma onto fused silica.[11] Photoinduced ablation of these samples could be observed, indicating a relatively smooth surface topography on the ablated areas. However, due to broadband reflectivity of the employed gold mirror, the influence of out-of-band radiation (especially from the higher UV and visible spectral range) could not be excluded.

In this paper we present first data on EUV direct photoetching obtained with a compact laser-produced EUV plasma source with an integrated EUV Schwarzschild objective.[12–14] Imaging of the laser plasma generated in a xenon gas target leads to a high EUV pulse energy density (approximately 75 mJ/cm^2, pulse width 6 ns) far away from the source, capable of structuring or modifying materials with micron resolution. Sample damage due to the influence of the hot plasma can be avoided, and, most important, the observed irradiation effects can be assigned to 13.5 nm radiation exclusively, since the Mo/Si multilayer mirror coatings of the Schwarzschild objective in combination with a zirconium filter are effectively blocking out-of-band radiation in the target plane.

Together with a description of the setup and characterization of the integrated EUV source and optics system, results on EUV-induced photoetching of PMMA are presented. Due to its optomechanical and chemical properties PMMA is an interesting candidate for micro-optical components like diffractive elements or waveguide structures,[15] as well as a photoresist for *e*-beam and EUV lithography.[16] Nevertheless,

[a]Electronic mail: fbarkusky@llg.gwdg.de

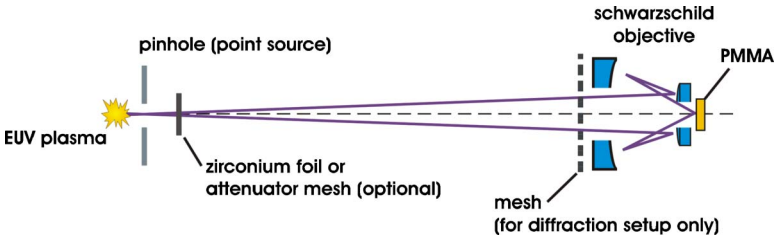

FIG. 1. Schematic drawing of the EUV source and optics system. The sample is mounted on a 3-axes translation stage. In order to achieve a flat-top EUV beam profile a 50 μm pinhole was positioned ~2 mm behind the plasma. Optional attenuation and spectral filtering is achieved using a mesh and/or a zirconium foil close to the pinhole. For diffraction experiments a mesh is placed near the objective.

the interaction processes between EUV radiation and PMMA, especially ablation and etching, are not well-examined yet.

On the other hand, ablation of PMMA has been investigated extensively at higher wavelengths, especially in the deep UV spectral range using excimer lasers,[17,18] where incubation effects at the beginning of the irradiation[18] as well as threshold energy densities for ablation[17] had been observed. The results on EUV etch rates presented below are discussed in comparison to the excimer laser data.

II. EXPERIMENTAL SETUP

A. EUV source

The experimental setup consists of a laser-based EUV source[12–14] and a separate optics chamber adapted to this source (cf. Fig. 1). EUV radiation is generated by focusing a Nd:YAG laser (Innolas, wavelength 1064 nm, pulse energy 700 mJ, and pulse length 6 ns) into a pulsed gas jet produced by an electromagnetically switched valve. The nozzle tip is located in the center of the vacuum chamber, which is evacuated to approximately 10^{-3} mbar to account for the low mean free path of EUV radiation at atmospheric pressure. The use of a laser-drilled conical nozzle guarantees a high particle density in the pulsed gas jet and, consequently, high quantum efficiency for EUV generation.[13] Xenon is employed as target gas, accomplishing broadband radiation in the wavelength range from 8 to 15 nm.[12] The plasma can be monitored with a pinhole camera, consisting of a charge coupled device (CCD) chip with an EUV-to-VIS quantum converter and a pinhole (diameter 30 μm) coated with a zirconium foil (thickness approximetely 200 nm) for blocking of out-of-band radiation.[14]

Table I shows selected properties of the employed EUV source as used in the described experiments.

B. Schwarzschild objective

The purpose of the employed EUV objective was to achieve a high EUV fluence in the focal plane by demagnified imaging of the source, combined with a high spatial resolution (several lines per micron) and a compact setup.

TABLE I. Output parameters of the laser-based EUV plasma source.

Wavelength (λ)	8–15 nm
Pulse width (τ)	6 ns
Energy (Q)	3 mJ (13.5 nm, 2%BW, 4π sr)
Plasma diameter (d)	300 μm (FWHM, nearly spherical)
Repetition rate (f_p)	1 Hz

Table II summarizes optical parameters and mechanical dimensions of the mirror design, which has been described already previously.[5] The alignment of the objective was performed at atmospheric pressure, using a Hartmann-Shack wave front sensor in the visible spectral range.[19,20] The dimensions of the entire EUV source and optics system including a laser, power supplies, gas bottle, and vacuum pump are $100\times60\times145$ cm^3 ($W\times D\times H$).

By imaging the EUV plasma directly, a theoretical energy density of about 73 mJ/cm^2 can be evaluated for an EUV source energy of 3 mJ and a source diameter of 300 μm. However, in order to generate a flat-top-like intensity profile, a pinhole (50 μm diameter) was positioned 2 mm behind the plasma and imaged by the objective.[5] Thus by translating the sample into the image plane of the pinhole, a writing spot of 5 μm diameter with steep edges is obtained. Due to the reduced fluence on the pinhole, the maximum energy density in the image plane is approximately two times smaller than for direct imaging of the plasma.

PMMA plates (Goodfellow, thickness 1 mm, standard grade) were used as irradiation targets. They were cleaned for 5 min in an ultrasonic ethanol bath before exposure.

III. RESULTS

Figure 2 shows first results of EUV photoetching from PMMA. Each spot was irradiated by 100 EUV pulses at a fluence of approximetely 35 mJ/cm^2 per pulse. The sample was displaced by 10 μm laterally and 3 μm on the optical axis between each spot, respectively. After exposure the sample was cleaned in ethanol to remove generated polymer fragments. The AFM micrograph in Fig. 2 (below) shows the spot with the steepest edges, indicating the image plane of the objective.

TABLE II. Specifications of EUV mirror objective and resulting focus parameters.

Distance source–image plane	520.5 mm
Magnification (M)	0.102
Numerical aperture (NA)	0.4
Acceptance angle (Ω)	5.33 msr
Reflectivity of Mo/Si mirror coatings (R)	>60% per mirror at 13.5 nm
Number of mirrors (n)	2
Spot size	~30 μm (source image) ~5 μm (imaging of 50 μm pinhole)
EUV energy density (H)	~73 mJ/cm^2 (source image) <37 mJ/cm^2 (imaging of 50 μm pinhole)

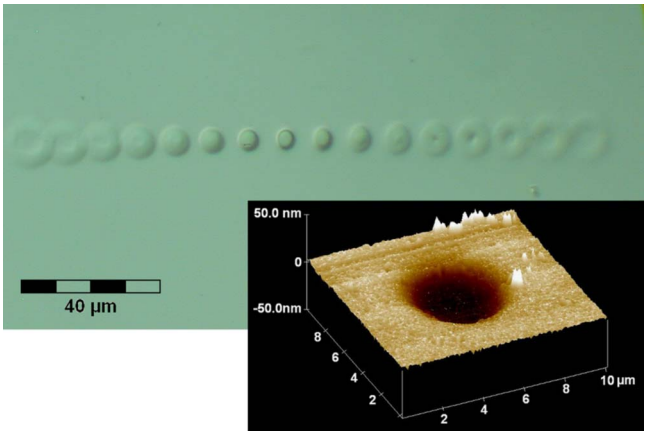

FIG. 2. (Top) Optical micrographs of EUV induced surface modification of PMMA for different sample positions (mask-imaging, cf. text). Each site was exposed to 100 EUV pulses (pulse energy density 37 mJ/cm^2, cleaning of surface with ethanol after exposure). The sample was displaced by 10 μm laterally and 3 μm on the optical axis between every two spots. (Bottom) AFM measurement of etched crater with steepest edges, indicating the correct image plane.

A. EUV energy density

In order to determine the correct EUV energy in the image plane, an EUV photodiode (AXUV-100, uncoated, IRD Inc.) was positioned behind the Schwarzschild objective. For spectral filtering a zirconium foil [thickness 220 nm, transmission 0.468 (CXRO)] is positioned near the EUV source. This foil is stabilized by a steel mesh with a transmission of 0.85. Furthermore, the radiation is filtered by the Mo/Si multilayer coatings of the objective. The employed multilayers (FhG-IOF/Jena) exhibit a high reflectance both at 13.5 nm [≥60%, 2% full width at half maximum (FWHM) of central wavelength] and in the vacuum ultraviolet (VUV) spectral range (>100 nm wavelength).[21] By use of an additional zirconium filter this unwanted out-of-band radiation can be blocked effectively.

Figure 3 shows the measured EUV energy of zirconium filtered radiation in the image plane as a function of the

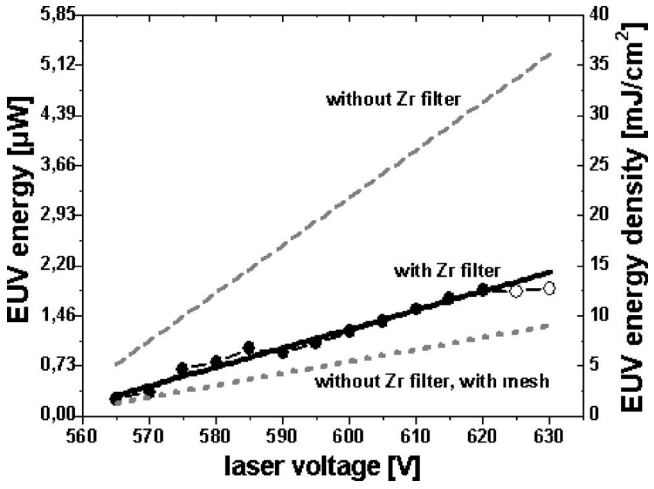

FIG. 3. EUV energy measured with a photodiode (AXUV100) in the image plane of the applied Schwarzschild objective vs laser voltage. The energy density was computed using the spot area determined from the caustic measurement in Fig. 2.

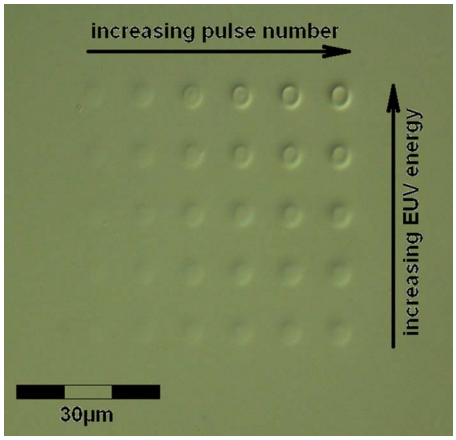

FIG. 4. Nomarski (DIC) micrograph of a PMMA sample irradiated with various pulse numbers (50–800, from left to right) and at different EUV energy densities (10–37 mJ/cm^2, from bottom to top). The distance between adjacent spots is 10 μm.

applied Nd:YAG laser lamp voltage, which is used to change the EUV source energy. Without zirconium filtering, the achievable EUV energy density is more than two times higher, leading, on the other hand, to out-of-band radiation in the image plane. The influence of this radiation on PMMA photoetching can be determined by comparing zirconium filtered and unfiltered radiation at comparable EUV energy densities. This was accomplished by attenuating unfiltered radiation with a stainless steel mesh (transmission approximately 0.25, cf. Fig. 1), leading to a wavelength-independent attenuation of the source radiation.

B. Determination of etch rates

For determination of etch rates as a function of EUV energy density different experiments were performed. Figure 4 shows the DIC micrograph of a PMMA sample irradiated by unfiltered EUV radiation. Every row was exposed to an increasing number of EUV pulses (50–800, from left to right) at constant EUV fluence, every column indicates a constant number of EUV pulses at increasing fluence (from 10 to 37 mJ/cm^2, bottom to top).

The depths of the generated ablation craters were determined by atomic force microscopy (Nanoscope III) in tapping mode. Figure 5 shows a compilation of the results obtained for unfiltered EUV radiation. At lower densities (below 10 mJ/cm^2) the crater depth is about proportional to the pulse number, whereas at higher densities nonlinearities are observed. These can, at least partly, be ascribed to deformations on the bottom of the crater, leading to an incorrect depth determination. The vaulted crater bottom can be explained by several different mechanisms. One is radiation-induced cross-linking of polymer chains, which could reduce the EUV etch rate of PMMA as discussed by Mocek *et al.*[22] Another possibility is the attenuation of the radiation by the gaseous fragments of PMMA, leading to absorption of the trailing edge of the incoming nanosecond EUV pulse. The nonuniform fragment density with a maximum in the center of the ablated area could lead to the observed crater shape. On the other hand, the plasma shielding effect known for

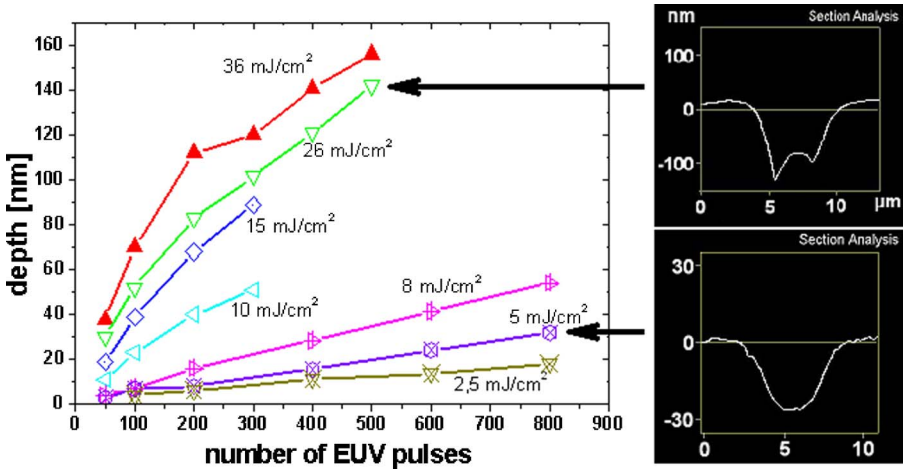

FIG. 5. Plot of etch depth versus number of pulses for different EUV energy densities (left). Below 10 mJ/cm^2 the depth is nearly proportional to the number of pulses. Above this value distortions of the ablation crater at higher pulse numbers impede the exact evaluation (right).

higher wavelengths (especially for excimer laser ablation[23]) cannot be taken into account because of a low electron density in the plume formed at the low fluence.

In order to investigate the influence of still existing out-of-band radiation, the experiment from Fig. 5 was repeated using an additional zirconium filter (cf. Fig. 1), leading to 13.5 nm radiation in the image plane exclusively (FWHM of 2%, limited by the reflectance of the Mo/Si mirrors). With this setup, EUV energy densities between 2 and 13 mJ/cm^2 can be obtained. Results are shown in Fig. 6. Both graphs show a nearly linear trend. Other than for corresponding excimer laser results,[17] there is obviously no indication of a threshold level in energy density. However, the etch rate for unfiltered radiation indicates a larger gradient than the zirconium filtered curve, which can be ascribed to the out-of-band radiation (see below).

C. EUV diffraction experiment

The influence of out-of-band radiation was investigated by conducting a diffraction experiment as described in the following: In order to generate a diffraction pattern in the target plane, a steel mesh with 25 μm wire diameter and a period of 50 μm was positioned 5 mm in front of the objective (Fig. 1). For this plane, the spatial coherence length of the EUV radiation emitted from the source can be calculated from the Van Zittert-Zernike theorem. For the existing special case of an incoherently illuminated pinhole positioned directly behind the plasma, the normalized spatial coherence between two points O and P in the plane of the mesh is given by[24]

$$\mu_{OP}(\theta) = e^{-i\psi}\frac{2J_1(ka\theta)}{ka\theta}, \tag{1}$$

where ψ is the phase variation between these points, J_1 is a Bessel function of the first kind of order one, k the wave number, a radius of the illuminated pinhole, and θ the angle between O and P as seen from the pinhole, respectively.

For a pinhole radius of 25 μm and a distance between pinhole and mesh of 385 mm, the spatial coherence length ($1/e$ decay) is approximately 85 μm. Therefore interference patterns originating from two mesh periods should be visible in the etched profile of an irradiated PMMA sample.

The actual experiments were performed both with Zr filtered and unfiltered radiation. In Fig. 7, left, an AFM image of the PMMA surface topography is shown after applying 2000 EUV pulses (pulse energy 1.02 μJ at 13.5 nm, unfiltered radiation). Clearly, a diffraction pattern is observed: besides the zeroth order, also the orders 1, 1.1, and even faint third order spots are visible, whereas the second diffraction order is suppressed. The lattice constant of the periodic etch profile was determined to approximately 10.9 μm.

In order to simulate this experimental result, standard diffraction theory[25] was applied, approximating the incident wave front as a plane wave for simplification. The corresponding computed diffraction pattern is shown in Fig. 7 (right), indicating good qualitative agreement with the experiment, as documented in particular by the absence of second order diffraction patterns. Taking the magnification of the mirror objective into account, the theoretical spacing between diffraction orders is 9.7 μm for 13.5 nm radiation. This fits well with the period obtained experimentally, proving the fact that the higher diffraction orders are indeed caused by EUV radiation.

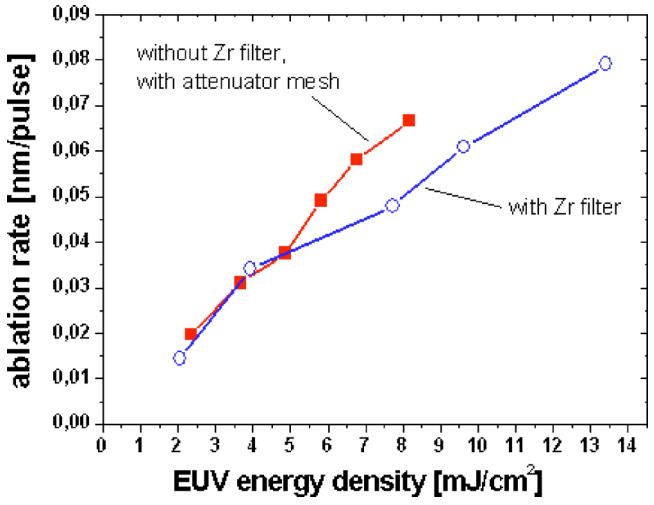

FIG. 6. PMMA etch rate as a function of EUV energy density. To obtain comparable energy densities the measurement without a Zr filter was performed with a stainless steel attenuator mesh (25 μm wire diameter, 50 μm period, transmission 25%).

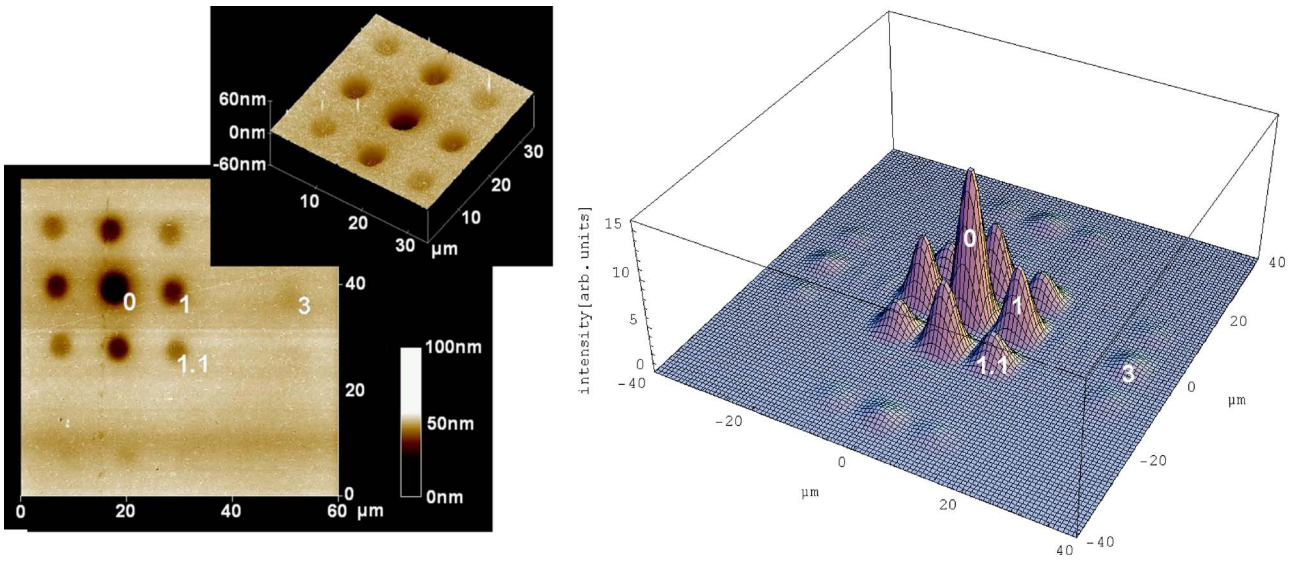

FIG. 7. Diffraction of EUV radiation from stainless steel mesh (20 lines/mm) positioned in the beam path (cf. Fig. 1). (Left) AFM measurement of PMMA site after irradiation with 2000 pulses. (Right) simulated intensity distribution in the image plane (cf. text).

For a quantitative determination of the influence of out-of-band radiation on PMMA photoetching, the depths of the generated diffraction orders obtained for filtered and unfiltered radiation are compared with the simulated intensities, assuming a linear relation between etch depth and the number of applied pulses (cf. Fig. 5). The result is shown in Fig. 8 (all patterns normalized to first diffraction order). Obviously, the diffraction pattern generated by filtered radiation correlates very well with the simulated intensity profile. The pattern generated without a Zr filter only fits for the higher orders, which are generated by 13.5 nm radiation exclusively due to the much higher diffraction angles for (higher wavelength) out-of-band radiation. In contrast, the measured zeroth order (which contains also out-of-band radiation) is approximately 25% higher than the simulated one. Obviously, despite spectral filtering of the incident radiation by the Mo/Si multilayer mirrors of the Schwarzschild objective, out-of-band radiation contributes by ~25% to the etch depth of PMMA. This could be explained by local heating of the sample due to out-of band-radiation, which leads to increased etch rates as demonstrated by Bartnik for etching of PTFE.[26]

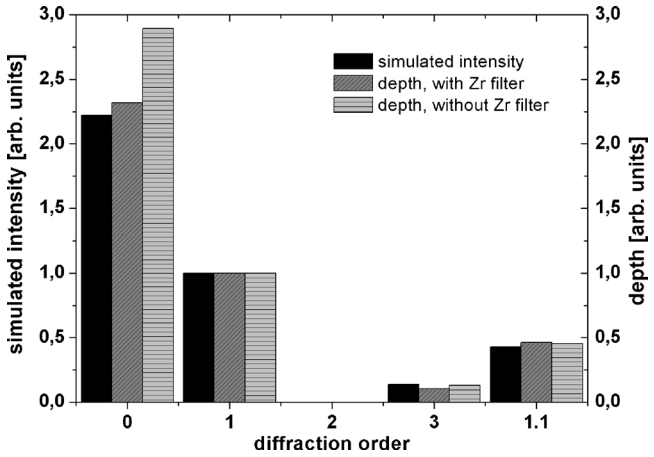

FIG. 8. Measured etch depths and simulated intensity of observed diffraction orders (both normalized to the first order). With Zr filter: only 13.5 nm radiation in the sample plane (±2% FWHM, 8000 pulses, pulse energy 0.47 μJ), without a Zr filter: radiation attenuated by stainless steel mesh, spectral filtering only by Mo/Si mirrors (EUV pulse energy 1.02 μJ, 2000 pulses).

D. Direct writing in PMMA

In order to demonstrate the possibility of direct writing of small structures in PMMA, the Schwarzschild objective was used in the mask imaging mode, with a 10 μm pinhole behind the plasma. By translating the sample laterally with a piezodriven manipulator, letters were written with an EUV spot of 1 μm diameter (cf. Fig. 9). The sample was moved approximately 1 μm between two positions, each site on the sample was exposed to 100 EUV pulses. The ablated area was visualized with the help of an AFM microscope.

IV. CONCLUSION

The observed PMMA surface modification presented in this paper can be assigned to 13.5 nm radiation exclusively due to the effective blocking of out-of-band radiation in the employed optical setup. For this reason, to our knowledge,

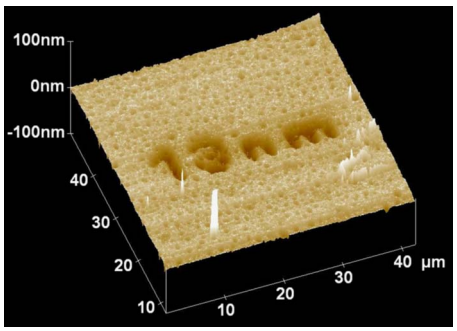

FIG. 9. Direct writing of structures in PMMA by direct photoetching with EUV radiation (AFM image). The EUV writing spot has a diameter of 1 μm. Each site was exposed to 100 pulses of approximately 25 mJ/cm^2.

the results represent the first systematic investigations on photoinduced etching in the EUV spectral range. Etch rates were determined to be in the range of 1 Å per EUV pulse at energy densities of 13 mJ/cm^2. In contrast to excimer laser ablation of PMMA with nanosecond pulses, neither an energy threshold nor the need for incubation pulses was observed. This can be ascribed to the much higher photon energy (92 eV for $\lambda = 13.5$ nm as compared to 5 eV for $\lambda = 248$ nm), strongly exceeding the bonding energy within the PMMA polymer (several eV); thus a single EUV photon is capable of breaking a large number of PMMA bonds.

At higher energy densities (up to 35 mJ/cm^2) etch rates could not be determined accurately since the bottom of the ablated crater exhibits a convex shape, leading to errors in the depth measurements. This effect could be ascribed to radiation-induced cross-linking of polymer chains, or, alternatively, to an inhomogeneous attenuation of the radiation by the gaseous PMMA fragments, leading to absorption of the trailing edge of the incoming nanosecond EUV pulse.

In order to analyze the contribution of "out-of-band" radiation (especially above a wavelength of 100 nm) to PMMA etching, rates were determined both with and without zirconium filtering. For unfiltered radiation the rates were found to be about 20%–30% higher due the influence of out-of-band radiation. This result was confirmed by a diffraction experiment; here, the spectral discrimination was not achieved by filtering, but by diffraction of the incident radiation from a periodic mesh positioned in front of the Schwarzschild objective. This leads to the formation of a pronounced diffraction pattern in the surface topography of the ablated PMMA sample. While the zeroth order of this structure is formed by the entire wavelength spectrum, the higher orders can be attributed to 13.5 nm radiation exclusively, as documented by the excellent agreement with the simulation.

In forthcoming experiments we will focus on EUV induced photoetching of other polymers, such as polyimide or PTFE. Moreover, since the spatial resolution of approximately 1 μm achieved at present is mainly limited by figure errors of the Schwarzschild objective, ion beam corrected mirror substrates will be employed in the near future in order to achieve a resolution in the range of 100 nm. At the same time, also the output characteristics of the table-top EUV source will be optimized with respect to both EUV pulse energy and repetition rate.

ACKNOWLEDGMENTS

The authors would like to thank T. Feigl from FhG-IOF (Jena/Germany) for deposition of the Mo/Si multilayer mirrors, as well as L. Juha (Czech Academy of Sciences/Prague) for fruitful discussions. The financial support by the Bundesministerium für Bildung und Forschung within the project "KOMPASS" (Kompakte Strahlquelle hoher Brillanz für den weichen Röntgen-Spektralbereich) is gratefully acknowledged.

[1] See, e.g., *SPIE Proceedings of "Microlithography," San Jose* (SPIE, 2005).
[2] T. Feigl, S. Yulin, N. Benoit, and N. Kaiser, Microelectron. Eng. **83**, 703 (2004).
[3] See *SPIE Proceedings of "Emerging Lithographic Technologies X," San Jose*, Vol. 6151 (SPIE, 2006).
[4] U. Stamm J. Phys. D **37**, 3244 (2004).
[5] F. Barkusky, K. Mann, C. Peth, T. Feigl, and N. Kaiser, Rev. Sci. Instrum. **76**, 105102 (2005).
[6] H. Gu and L. Qi, Opt. Commun. **210**, 299 (2002).
[7] E. J. Caine and S. D. Miller, J. Vac. Sci. Technol. B **16**, 3232 (1998).
[8] G. Baldacchini, S. Bollanti, F. Bonfigli, P. Di Lazzaro, A. Y. Faenov, F. Flora, T. Marolo, R. M. Montereali, D. Murra, E. Nichelatti, T. Pikuz, A. Reale, L. Reale, A. Ritucci, and G. Tomassetti, IEEE J. Sel. Top. Quantum Electron. **10**, 1435 (2004).
[9] L. Juha, J. Krasa, A. Prag, A. Cejnarova, D. Chvostova, K. Rohlena, K. Jungwirth, J. Kravarik, P. Kubes, Y. L. Bakshaev, A. S. Chernenko, V. D. Korolev, V. I. Tumanov, M. I. Ivanov, A. Bernardinello, J. Ullschmied, and F. P. Boody, Surf. Rev. Lett. **9**, 347 (2002).
[10] H. Fiedorowicz, A. Bartnik, M. Bittner, L. Juha, J. Krasa, P. Kubat, J. Mikolajczyk, and R. Rakowski, Microelectron. Eng. **73–74**, 336 (2004).
[11] T. Makimura, Y. Kenmotsu, H. Miyamoto, H. Niino, and K. Murakami, Surf. Sci. **593**, 248 (2005).
[12] S. Kranzusch and K. Mann, Opt. Commun. **200**, 223 (2001).
[13] C. Peth, S. Kranzusch, K. Mann, and W. Viöl, Rev. Sci. Instrum. **75**, 3288 (2004).
[14] S. Kranzusch, C. Peth, and K. Mann, Rev. Sci. Instrum. **74**, 969 (2003).
[15] J. S. Koo, P. G. R. Smith, R. B. Williams, C. Riziotis, and M. C. Grossel, Opt. Mater. **23**, 583 (2003).
[16] D. He, H. Solak, and F. Cerrina, J. Vac. Sci. Technol. B **17**, 3379 (1999).
[17] G. B. Blanchet, Macromolecules **28**, 4603 (1995).
[18] R. Srinivasan, B. Braren, and K. G. Casey, J. Appl. Phys. **68**, 1842 (1990).
[19] B. Schäfer and K. Mann, Appl. Opt. **41**, 2809 (2002).
[20] B. Schäfer and K. Mann, Rev. Sci. Instrum. **71**, 2663 (2000).
[21] Homepage of Center for X-Ray Optics, Berkeley Lab, X-Ray Interaction with Matter Calculator; http://www.cxro.lbl.gov/
[22] T. Mocek, B. Rus, M. Stupka, M. Kozlová, A. R. Präg, J. Polan, M. Bittner, R. Sobierajski, and L. Juha, Appl. Phys. Lett. **89**, 051501 (2006).
[23] A. P. Ghosh and J. E. Hurst, J. Appl. Phys. **64**, 287 (1988).
[24] D. Attwood, *Soft X-rays and Extreme Ultraviolet Radiation–Principles and Applications* (University of California and Lawrence Berkeley National Laboratory, Cambridge, 2000), pp. 321–330.
[25] E. Hecht, in *Optics*, 2nd ed. (Addison-Wesley, Reading, MA, 1987).
[26] A. Bartnik, H. Fiedorowicz, R. Jarocki, L. Juha, J. Kostecki, R. Rakowski, and M. Szczurek, Appl. Phys. B **82**, 529 (2006).